



Symbolic Computation of Local Stability and Bifurcation Surfaces for Nonlinear Time-Periodic Systems

E. A. BUTCHER and S. C. SINHA

Nonlinear Systems Research Laboratory, Department of Mechanical Engineering, Auburn University, Auburn, AL 36849, U.S.A.

(Received: 20 June 1997; accepted: 14 April 1998)

Abstract. A new technique is presented for symbolic computation of local stability boundaries and bifurcation surfaces for nonlinear multidimensional time-periodic dynamical systems as an explicit function of the system parameters. This is made possible by the recent development of a symbolic computational algorithm for approximating the parameter-dependent fundamental solution matrix of linear time-periodic systems. By evaluating this matrix at the end of the principal period, the parameter-dependent Floquet Transition Matrix (FTM), or the linear part of the Poincaré map, is obtained. The subsequent use of well-known criteria for the local stability and bifurcation conditions of equilibria and periodic solutions enables one to obtain the equations for the bifurcation surfaces in the parameter space as polynomials of the system parameters. Further, the method may be used in conjunction with a series expansion to obtain perturbation-like expressions for the bifurcation boundaries. Because this method is *not* based on expansion in terms of a small parameter, it can be successfully applied to periodic systems whose internal excitation is strong. Also, the proposed method appears to be more efficient in terms of *cpu* time than the truncated point mapping method. Two illustrative example problems, *viz.*, a parametrically excited simple pendulum and a double inverted pendulum subjected to a periodic follower force, are included.

Keywords: Symbolic computation, stability, bifurcation, nonlinear, time-periodic.

1. Introduction

The study of dynamical systems governed by a set of nonlinear ordinary differential equations with periodic coefficients is of great theoretical and practical importance in various fields of science and engineering. Equilibria and periodic solutions of these equations physically represent steady-state operations under various conditions. The stability and bifurcation of these solutions is determined by the equations of perturbed motion about the equilibrium or periodic solution. Hence, a set of time-periodic quasilinear equations generally arise from the Taylor series expansion about these solutions. The stability and bifurcation conditions are determined from the eigenvalues of the linearized system's fundamental solution matrix evaluated at the end of the principal period (called the Floquet Transition Matrix (FTM)) in much the same way as the eigenvalues of a linear system matrix determine the stability of time-invariant systems. Similar to the Routh–Hurwitz criteria for time-invariant systems, various well-known criteria may be used to extract the parameter-dependent stability and bifurcation relations of the time-periodic system from the FTM provided that this matrix can be symbolically obtained in terms of the system parameters.

It is well known that exact solutions of periodic systems are possible only in a very limited number of cases, and, in general such solutions do not exist. Two common analytical methods that have been used in the past to yield approximate stability boundaries in closed form for small systems include the perturbation method [1] and the averaging technique [2]. These

methods are limited in application to systems with weak internal excitation since they are based on expanding the solution in terms of a small parameter that multiplies the time-periodic terms. When the excitation becomes strong, the parameter is not small and the accuracy of the solution is very poor. Moreover, increasing the order of the approximate solution is usually very difficult and does not guarantee uniform convergence to the true solution. Other methods such as Hill's infinite determinants [3] are not computationally convenient for large order systems and, in addition, may not be applicable for bifurcations to quasiperiodic solutions. A recent approximation technique of Guttalu and Flashner [4, 5] for computing the FTM, or the linearized Poincaré map, by truncated point mappings employs a variation of the standard Runge–Kutta numerical integration technique adapted to symbolic computation. By avoiding the restriction of a small periodic parameter, it thus allows the computation of stability and bifurcation surfaces for internal excitation of arbitrary strength. From the results reported by the authors, however, it appears that the method could be computationally expensive for relatively large systems [5]. This is due to the nature of the algorithm, which involves the truncation of polynomials at a fixed degree after performing a symbolic matrix multiplication at each integration step.

Another technique to approximate the parameter-dependent FTM, which has been developed recently, involves the use of Picard iteration and expansion of the time-periodic system matrix in shifted Chebyshev polynomials. This technique, which was introduced by Sinha and Butcher [6], results in an algorithm to compute the fundamental solution matrix explicitly as a function of the system parameters and time and is easily implemented using symbolic software such as Mathematica since it involves only simple matrix multiplications and additions. This is done by employing the *integration* and *product operational matrices* associated with the polynomials used in previous studies for numerical computations by Sinha and Wu [7]. By evaluating the fundamental solution matrix at the end of the principal period, the parameter-dependent FTM is obtained. The subsequent use of well-known criteria for the local stability and bifurcation conditions of equilibria and periodic solutions enables one to obtain the equations for the bifurcation surfaces in the parameter space. Since these equations are expressed as homogeneous polynomials of the system parameters, they can be solved for one parameter once values of the others have been chosen. As with truncated point mappings, this method can successfully be applied to periodic systems with strong internal excitations since it does *not* involve expansion in terms of a small parameter. Nevertheless, the perturbation expansions may also be derived via a series substitution. Results demonstrate that the proposed technique appears to be faster in terms of *cpu* time than the truncated point mapping method while providing an equivalent accuracy. Two illustrative example problems, viz., a parametrically excited simple pendulum and a double inverted pendulum subjected to a periodic follower force, are included, and the results are discussed in detail.

2. Local Stability and Bifurcation of Time-Periodic Systems

Consider a dynamical system described by the set of N nonlinear ordinary differential equations

$$\dot{\mathbf{y}}(t) = \mathbf{f}(\mathbf{y}(t), t, \boldsymbol{\alpha}) = \mathbf{f}(\mathbf{y}(t), t + T, \boldsymbol{\alpha}), \quad \mathbf{y}(0) = \mathbf{y}^0, \quad (1)$$

where $t \in \mathbb{R}^+$ denotes time, $\mathbf{y} \in \mathbb{R}^N$ is the state vector, $\boldsymbol{\alpha} \in \mathbb{R}^L$ is a vector of control parameters, and $\mathbf{f} : \mathbb{R}^+ \times \mathbb{R}^N \times \mathbb{R}^L \rightarrow \mathbb{R}^N$ is analytic in the components of \mathbf{y} and $\boldsymbol{\alpha}$ and periodic

in t with period T . Let $\bar{\mathbf{y}}(t)$ denote a known equilibrium or periodic solution of period KT of Equation (1) and $\mathbf{x}(t) = \mathbf{y}(t) - \bar{\mathbf{y}}(t)$, a perturbation about this solution. Expanding Equation (1) in Taylor series about $\bar{\mathbf{y}}(t)$ yields

$$\begin{aligned} \dot{\mathbf{x}} = & \mathbf{A}(t, \boldsymbol{\alpha})\mathbf{x} + \mathbf{f}_2(\mathbf{x}, t, \boldsymbol{\alpha}) + \mathbf{f}_3(\mathbf{x}, t, \boldsymbol{\alpha}) + \dots \\ & + \mathbf{f}_k(\mathbf{x}, t, \boldsymbol{\alpha}) + O(|\mathbf{x}|^{k+1}), \quad \mathbf{x}(0) = \mathbf{x}^0 = \mathbf{y}^0 - \bar{\mathbf{y}}(0), \end{aligned} \quad (2)$$

where $\mathbf{f}_k(\cdot)$ contain homogeneous monomials in x_i of order k , and $\mathbf{A}(t, \boldsymbol{\alpha})$ and $\mathbf{f}_k(\mathbf{x}, t, \boldsymbol{\alpha})$ are periodic in t with period KT where $K = 1$ if $\bar{\mathbf{y}}(t)$ is an equilibrium position.

We are interested in obtaining the local stability and bifurcation conditions of Equation (2) as a function of the system parameters. For this purpose, the linear part of Equation (2) given by

$$\dot{\mathbf{x}} = \mathbf{A}(t, \boldsymbol{\alpha})\mathbf{x}, \quad \mathbf{x}(0) = \mathbf{x}^0 \quad (3)$$

is now considered.

If the linearized system is *hyperbolic*, then the local stability of Equation (2) is given completely by the eigenvalues (Floquet multipliers) μ_i of the Floquet Transition Matrix (FTM)

$$\mathbf{H}(\boldsymbol{\alpha}) = \Phi(KT, \boldsymbol{\alpha}), \quad (4)$$

where $\Phi(t, \boldsymbol{\alpha})$ is the fundamental solution matrix associated with Equation (5). The stability condition can be expressed as $|\mu_i| < 1, i = 1, 2, \dots, N$; that is, all multipliers must lie within the unit circle in the complex plane. If one or more multipliers lie directly on the circle, the system is *nonhyperbolic*, and even if the remaining multipliers remain inside the circle, the linear analysis is inconclusive. In this case the stability conditions may be obtained by reducing Equation (4) on the center manifold [8]. If any of the multipliers lie outside the unit circle, then Equation (1) is locally unstable in the neighborhood of $\bar{\mathbf{y}}(t)$ although the question of its global stability remains open. It should be noted that, due to additional symmetry requirements, Hamiltonian systems are stable only when all of the multipliers lie on the unit circle [9].

The bifurcation route associated with Equation (2) depends on whether the Floquet multipliers cross the unit circle at $+1, -1$, or as pairs of complex numbers. The three generic codimension 1 bifurcations which can occur are [10]: (i) *fold* bifurcation to a period KT solution, which implies $\det(\mathbf{I} - \mathbf{H}(\boldsymbol{\alpha})) = 0$ since $\mu_i = 1$ for some $i \in [1, \dots, N]$; (ii) *flip* bifurcation to a period $2KT$ solution, which implies $\det(\mathbf{I} + \mathbf{H}(\boldsymbol{\alpha})) = 0$ since $\mu_i = -1$; and (iii) *secondary Hopf*, for which $|\mu_i| = |\mu_i^*| = 1$. For a single degree-of-freedom system the condition for the latter bifurcation is simply $\det(\mathbf{H}(\boldsymbol{\alpha})) = 1$. If the system is Hamiltonian, this condition is satisfied automatically since $\mathbf{H}(\boldsymbol{\alpha})$ is a symplectic map, and, therefore, destabilization occurs only via *tangent* and *period-doubling* (the Hamiltonian version of fold and flip) bifurcations when $\text{tr}(\mathbf{H}(\boldsymbol{\alpha})) = +2$ or -2 , respectively. In these bifurcations, a single pair of Floquet multipliers meets on the unit circle at $+1$ or -1 , respectively, and then splits symmetrically along the real axis. Only in higher dimensional Hamiltonians is the *Krein collision* (also called the Hamiltonian Hopf bifurcation) possible [11] since two pairs of complex multipliers are required to meet on the unit circle before splitting.

3. Symbolic Computation of the Floquet Transition Matrix

Sinha and Butcher [6] have outlined a technique for computing the fundamental solution matrix $\Phi(t, \boldsymbol{\alpha})$ for a linear time-periodic dynamical system explicitly as a function of the system

parameters and time via Picard iteration and expansion in shifted Chebyshev polynomials. When this matrix is evaluated at the end of the principal period the Floquet transition matrix $\mathbf{H}(\boldsymbol{\alpha})$ is obtained. Hence the local stability and bifurcation conditions can be derived in a closed form. Sinha and Butcher outlined two formulations: one applicable to general time-periodic systems and the other for systems in which the periodic linear system matrix contains constant terms. It was shown that the latter restricts the set of parameters that can be used in the solution but converges much faster than does the former formulation. Only the first formulation (for general time-periodic systems) was utilized in this study.

The method is based on expressing the linear system (cf., Equation (3)) in the equivalent integral form

$$\mathbf{x}(t) = \mathbf{x}^0 + \int_0^t \mathbf{A}(\tau, \boldsymbol{\alpha}) \mathbf{x}(\tau) d\tau \quad (5)$$

and employing Picard iteration to find the $(k + 1)$ th approximation

$$\begin{aligned} \mathbf{x}^{(k+1)}(t) &= \mathbf{x}^0 + \int_0^t \mathbf{A}(\tau_k, \boldsymbol{\alpha}) \mathbf{x}^{(k)}(\tau_k) d\tau_k \\ &= \left[\mathbf{I} + \int_0^t \mathbf{A}(\tau_k, \boldsymbol{\alpha}) d\tau_k + \int_0^t \mathbf{A}(\tau_k, \boldsymbol{\alpha}) \int_0^{\tau_k} \mathbf{A}(\tau_{k-1}, \boldsymbol{\alpha}) d\tau_{k-1} d\tau_k \right. \\ &\quad \left. + \cdots + \int_0^t \mathbf{A}(\tau_k, \boldsymbol{\alpha}) \cdots \int_0^{\tau_1} \mathbf{A}(\tau_0, \boldsymbol{\alpha}) d\tau_0 \cdots d\tau_k \right] \mathbf{x}^0, \end{aligned} \quad (6)$$

where τ_0, \dots, τ_k are all dummy variables. The expression in brackets is an approximation to the fundamental solution matrix since it is truncated after a finite number of terms (iterations). After the period is normalized to 1 via the transformation $t = KT\tau$, the normalized 1-periodic system matrix $\bar{\mathbf{A}}(\tau, \boldsymbol{\alpha}) = \bar{\mathbf{A}}(\tau + 1, \boldsymbol{\alpha})$ is expanded in m shifted Chebyshev polynomials of the first kind valid in the interval $[0, 1]$ as

$$\bar{\mathbf{A}}(\tau, \boldsymbol{\alpha}) = \hat{\mathbf{T}}^T(\tau) \mathbf{D}(\boldsymbol{\alpha}), \quad (7)$$

where $\hat{\mathbf{T}}^T(\tau)$ is the $N \times Nm$ Chebyshev polynomial matrix and $\mathbf{D}(\boldsymbol{\alpha})$ is the $Nm \times N$ Chebyshev coefficient matrix. When this is inserted into Equation (12), the integration and product operational matrices [7] associated with the Chebyshev polynomials may be employed to achieve an expression for the expansion of $\Phi(t, \boldsymbol{\alpha})$ in shifted Chebyshev polynomials as

$$\Phi^{(p,m)}(\tau, \boldsymbol{\alpha}) = \hat{\mathbf{T}}^T(\tau) \left[\hat{\mathbf{I}} + \left(\sum_{k=1}^p [\mathbf{L}(\boldsymbol{\alpha})]^k \right) \mathbf{P}(\boldsymbol{\alpha}) \right] = \hat{\mathbf{T}}^T(\tau) \mathbf{B}(\boldsymbol{\alpha}), \quad (8)$$

where the $Nm \times N$ Chebyshev coefficient matrix $\mathbf{B}(\boldsymbol{\alpha})$ is expressed in terms of $\hat{\mathbf{I}}$, $\mathbf{L}(\boldsymbol{\alpha}) = \hat{\mathbf{G}}^T \hat{\mathbf{Q}}_D(\boldsymbol{\alpha})$, and $\mathbf{P}(\boldsymbol{\alpha}) = \hat{\mathbf{G}}^T \mathbf{D}(\boldsymbol{\alpha})$. Additional details on this algorithm, including the operational matrices $\hat{\mathbf{I}}$, $\hat{\mathbf{G}}$ and $\hat{\mathbf{Q}}_D$ and the ‘alternate formulation’, are given in [6].

It should be observed that the form of Equation (8) is well suited for symbolic manipulation and that, unlike traditional perturbation or averaging, the technique is *not* based on

expansion in terms of a small parameter. Instead, all parameters are treated equally in Picard iteration so that the convergence is radial in the parameter space. By selecting the number p of Picard iterations (which determines the number of matrix multiplications employed in Equation (8) and the number m of polynomials (which determines the sizes of the matrices), this truncated expression gives an approximate solution to any desired degree of accuracy. When the resulting expression is evaluated at $\tau = 1$ ($t = KT$), the Floquet transition matrix $\mathbf{H}(\boldsymbol{\alpha}) = \Phi(KT, \boldsymbol{\alpha})$ is obtained where, similar to truncated point mapping, each individual matrix element is expressed as a P th degree homogeneous polynomial of the system parameters. However, unlike the truncated point mapping technique, the solution is also obtained explicitly as a function of time. In truncated point mapping the parametrically dependent FTM is ‘numerically integrated’ using a modified version of the Runge–Kutta algorithm with a preset time step h and polynomial degree P . Since from 100 to 200 time steps are usually needed for sufficient accuracy, no less than this many matrix multiplications are also required. Consequently, the polynomials are usually truncated with terms of degree higher than P discarded at each time step past the point where a P th degree polynomial is first achieved. In the present technique P increases with the number p of Picard iterations in a manner which is determined by the number of appearances of the parameters in the linear system matrix. For the two examples discussed in this study this relationship is $P = p/2$, while in [6] it was found to be $P = p$ for a commutative system. Once this relationship is known, p may be appropriately chosen to yield polynomials of any desired degree, and no truncation is necessary. The number of required matrix multiplications is generally less in the present method than in truncated point mapping, while the sizes of the matrices being multiplied are generally larger because of the required Chebyshev expansion. When these factors are weighed against one another, however, it turns out that the present technique may require less *cpu* time (as shown in Section 6) while the amount of memory required may be significantly higher than in the truncated point mapping technique.

4. Examples

4.1. A PARAMETRICALLY EXCITED SIMPLE PENDULUM

As an example of a single degree-of-freedom system, a parametrically forced simple damped pendulum is considered. It is assumed that the support of the pendulum (mass M , length L) is subjected to a sinusoidal motion in the vertical direction with amplitude A and frequency ω . The dimensionless equation of motion for the system is given by Flashner and Hsu [12] as

$$\ddot{\theta} + 2\xi\alpha\dot{\theta} + (\alpha^2 - \beta \sin 2\hat{t}) \sin \theta = 0 \tag{9}$$

where $\alpha = 2(\omega_n/\omega)$, $\beta = 4(A/L)$, $\omega_n^2 = g/L$, $c/(ML^2) = 2\xi\omega_n$, and $2\hat{t} = \omega t$. Denoting $x_1 = \theta$, $x_2 = \dot{\theta}$, and expanding $\sin \theta$ in a Taylor series about the vertical $\theta = 0$ equilibrium position, the above equation may be written in state space form as

$$\begin{pmatrix} \dot{x}_1 \\ \dot{x}_2 \end{pmatrix} = \begin{bmatrix} 0 & 1 \\ -(\alpha^2 - \beta \sin 2\hat{t}) & -2\xi\alpha \end{bmatrix} \begin{pmatrix} x_1 \\ x_2 \end{pmatrix} + \begin{pmatrix} 0 \\ -(\alpha^2 - \beta \sin 2\hat{t})(-x_1^3/6 + x_1^5/120 - \dots) \end{pmatrix}. \tag{10}$$

Letting $\alpha^2 = a$, $-\beta = 2b$, $2\xi\alpha = d$, $2\hat{t} = 2t + \pi/2$, and truncating the nonlinear terms, Equation (10) reduces to the damped linear Mathieu equation investigated in [5].

$$\begin{pmatrix} \dot{x}_1 \\ \dot{x}_2 \end{pmatrix} = \begin{bmatrix} 0 & 1 \\ -(a + 2b \cos 2t) & -d \end{bmatrix} \begin{pmatrix} x_1 \\ x_2 \end{pmatrix}. \quad (11)$$

For $d = 0$ the system is Hamiltonian and preserves volume in state space since $\text{tr}(\mathbf{A}(t, a, b)) = 0$ where $\mathbf{A}(t, a, b)$ is the linear system matrix. The Floquet transition matrix $\mathbf{H}(a, b)$ was symbolically approximated in terms of the two remaining system parameters for three different combinations of the number p of Picard iterations and the number m of Chebyshev polynomials via Equation (8). It was found that all four elements of $\mathbf{H}(a, b)$ are of order $\mathbf{O}(a^P b^P)$ where $P = p/2$, that is they consist of various powers of $a^i b^j$ up to degree $p/2$ such that $I + j \leq P$, $I = 0, \dots, P$, $j = 0, \dots, P$. A few leading terms of the elements of $\mathbf{H}(a, b)$ are given to the fourth decimal place as

$$\begin{aligned} \mathbf{H}_{11} &= \mathbf{H}_{22} = 1.0 - 4.9348 * a + 4.0587 * a^2 - 2.4674 * b^2 - 1.3353 * a^3 \\ &\quad + 1.5913 * a * b^2 + \dots, \\ \mathbf{H}_{12} &= 1.0 - 1.6449 * a + b + 0.8117 * a^2 - 0.6449 * a * b - 0.1350 * b^2 \\ &\quad - 0.1908 * a^3 + 0.1668 * a^2 * b + 0.0928 * a * b^2 - 0.0239 * b^3 + \dots, \\ \mathbf{H}_{21} &= -9.8696 * a + 16.2348 * a^2 + 9.8696 * a * b - 4.9348 * b^2 - 8.0116 * a^3 \\ &\quad - 6.3652 * a^2 * b + 8.2158 * a * b^2 + 4.9348 * b^3 + \dots. \end{aligned} \quad (12)$$

It should be noted that, although these computations were performed in floating point form (which is more efficient than rational fraction form), the diagonal elements in Equation (12) agree with those obtained in [5] while \mathbf{H}_{12} and \mathbf{H}_{21} differ by a factor of $T = \pi$ and $1/T$, respectively, which is a result of the scheme used to normalize the period to 1. The determinant of the FTM ($1.0 + \mathbf{O}(10^{-9})$) is very close to unity as required for the conservation of phase space volume in the Hamiltonian case.

The lines in the (a, b) plane where destabilization occurs in the linear system (Equation (11)) correspond to the bifurcation boundaries in the original nonlinear system and can be obtained by setting $\text{tr}(\mathbf{H}(a, b)) = \pm 2$. Substituting values for b results in polynomial equations for a which can be numerically solved to yield the stability boundaries as a list of points or as a curve through these points. The former method (list of points) was used to compute the boundaries shown in Figure 1 where $\mathbf{H}(a, b)$ was computed using (A) $(p, m) = (16, 13)$, (B) $(p, m) = (32, 20)$, (C) $(p, m) = (50, 32)$, and (D) direct numerical integration of Equation (11) for 234,800 points in the parameter plane. It can be seen that the convergence of the present method decreases radially from the origin as the familiar stability boundaries break up into extraneous lines when convergence is lost. This is in contrast to the convergence of classical averaging or perturbation which decreases with an increase in the periodic parameter alone. Furthermore, the symbolically approximated boundaries converge into agreement with the numerically integrated diagram as the number of iterations and polynomials are increased. While the computations in (A) and (B) were performed using MATHEMATICA on a SUN SPARC 20 with 128 MB of RAM, this amount of memory was found to be insufficient for the computations in case (C) for which a similar machine with additional memory (512 MB) was used. Because of problems which prohibit the accurate determination of the memory

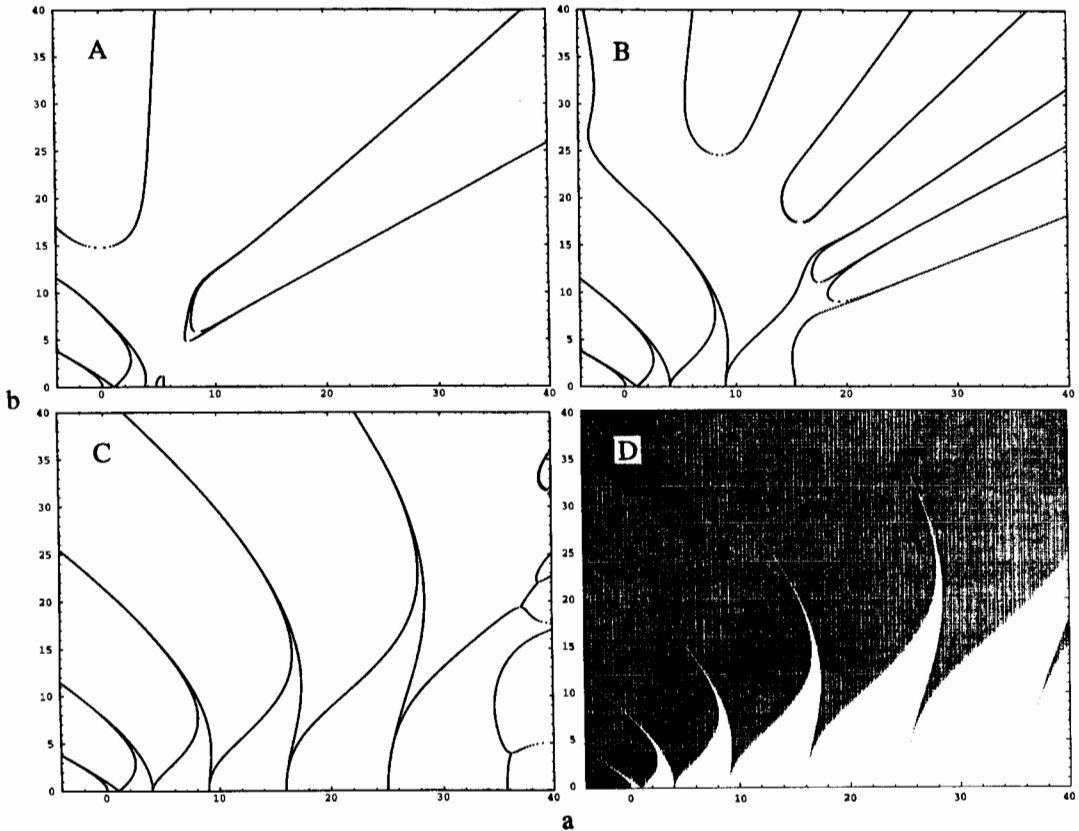


Figure 1. Stability boundaries for the Mathieu Equation computed symbolically with $(p, m) =$ (A) (16, 13), (B) (32, 20), (C) (50, 32), and (D) by direct numerical integration over one period. The white regions in the numerical diagram are stable and the black regions are unstable.

requirements, this information provides the best available measure of the amount of required memory. The required *cpu* times for various stages in computing the stability boundaries for each (p, m) set are given in Table 1. When the cumulative *cpu* time required to generate the stability boundaries using 8th degree polynomials in a and b is compared to the time required to generate the same 8th polynomial degree results with truncated point mappings using MATHEMATICA on a SPARC SERVER 1000 (reported in [5]), it is seen that truncated point mappings requires about seven times more *cpu* time than the present technique since these two machines are generally close in terms of speed. (The difference is approximately 15% or less.) It should be mentioned that *cpu* times (of 9 sec) for truncated point mapping using FORTRAN programs were also reported in [5] which, because a nonsymbolic code was utilized, require only 0.3 and 2% of the times required by MATHEMATICA based point mapping and the present technique, respectively. For additional information on how the *cpu* time varies with p in this problem, see [6]. A comparison of the $b = 0$ crossings for the two destabilization routes is also given in Table 1 where it is seen that the approximated crossings converge to the exact ones with an increase in number of iterations and polynomials. Furthermore, it has been shown in [5] and elsewhere that the results obtained from a perturbation analysis diverge rapidly with an increase in the periodic parameter and that convergence to the true boundaries is not guaranteed by increasing the order of the expansion.

Table 1. A comparison of efficiency and accuracy between the proposed symbolic algorithm and truncated point mappings (taken from Guttalu and Flashner [5]) in computing stability boundaries for Mathieu Equation.

	(p, m)	Present Technique			Truncated Point Mapping	
		(16, 13)	(32, 20)	(50, 32)	$N_t = 100$	$N_t = 100$
	polynomial degree P	8	16	25	8 (truncated)	32 (truncated)
Cumulative <i>cpu</i> time for computing	Chebyshev coefficients	0 h 04 m 47 s	1 h 30 m 46 s	~26 h	–	–
	$\mathbf{H}(a, b)$	0h 05m 24 s	1 h 46 m 0 s	~40h	–	–
	stability boundaries	0 h 07 m 15 s	7 h 06 m 19 s	~48 h	0 h 53 m 0 s	–
$b = 0$	tangent	0.000000	0.000000	0.000000		0.000000
intersections on a -axis computed from $\text{tr}(\mathbf{H}(a, 0)) = \pm 2$	stabilization	(3.756596;	4.000004	4.000005	–	4.000001
	exact: 0, 4, 16, 36	4.720525)	15.333822	16.000193		16.000066
	period-doubling	(0.999999	1.000000	1.000000		1.000000
	destabilization	$\pm 0.000331i$	(8.999970	9.000064	–	9.000012
	exact: 1, 9, 25		$\pm 0.005563i$)	(24.993257;		(25.000251
				25.006890)		$\pm 0.000033i$)

In addition, a first order averaging of Equation (11) yields unstable solutions only near the primary 2 : 1 resonance at $a = 1$ at which point the stability boundaries are equivalent to the first order (linear) perturbation approximation [13]. Higher order averaging is required to detect instability at the other resonance zones to the right. In contrast, the two parameters are treated equally in the present technique in which the use of a sufficiently high degree polynomial in a and b detects all unstable regions within a given radius from the origin.

The present method may also be used in conjunction with a series expansion in terms of the periodic parameter to recover the perturbation result. For this purpose, a is expanded in b as

$$a(b) = a_0 + \sum_{i=1}^q a_i b^i, \quad (13)$$

where a_0 is the $b = 0$ bifurcation point on the a axis from Table 1 and a_i are the expansion coefficients to be determined. Substituting Equation (13) into $\text{tr}(\mathbf{H}(a, b))$ and setting the expression equal to $+2$ or -2 (depending on whether a_0 corresponds to a tangent or period doubling bifurcation route, respectively), one then obtains q equations in the unknown coefficients a_i after collecting like powers of b . Since only one additional unknown coefficient

Table 2. A comparison of expansion coefficients for the tangent (fold) bifurcation boundary through $a = 0$ using the perturbation method and the proposed symbolic technique in conjunction with a series expansion for the parametrically-excited simple pendulum.

a_1	Perturbation ($d = 0$)	Present Technique ($d = 0$)	Present Technique ($d = 0.31623$)
a_1	0.0	0.0	0.0
a_2	-0.5	-0.5	-0.4878215567
a_3	0.0	0.0	0.0
a_4	5.46875×10^{-2}	$5.46874995 \times 10^{-2}$	$4.95841383 \times 10^{-2}$
a_5	0.0	0.0	0.0
a_6	$-1.2586805 \times 10^{-2}$	$-1.25868075 \times 10^{-2}$	$-1.048159919 \times 10^{-2}$
a_7	0.0	0.0	0.0
a_8	$3.63916821 \times 10^{-3}$	$3.63916923 \times 10^{-3}$	$2.768863617 \times 10^{-3}$
a_9	0.0	0.0	0.0
a_{10}	$-1.17976189 \times 10^{-3}$	$-1.17976235 \times 10^{-3}$	$-8.177643289 \times 10^{-4}$
a_{11}	0.0	0.0	0.0
a_{12}	$4.09943800 \times 10^{-4}$	$4.09944004 \times 10^{-4}$	$2.584121933 \times 10^{-4}$
a_{13}	0.0	0.0	0.0
a_{14}	$-1.49258328 \times 10^{-4}$	$-1.49258417 \times 10^{-4}$	$-8.546138625 \times 10^{-5}$
a_{15}	0.0	0.0	0.0
a_{16}	$5.62024774 \times 10^{-5}$	$5.62025166 \times 10^{-5}$	$2.920567178 \times 10^{-5}$

is introduced in any successive equation, one must solve q linear equations successively to recover the perturbation series which is then given by Equation (13). This was done to up 16th order for the tangent bifurcation route at $a_0 = 0$ and the resulting a_i coefficients are presented in Table 2 along with the exact perturbation coefficients given by McLachlan [14] in decimal notation. These results may also be expressed in the rational fraction notation, most common in perturbation analysis, as

$$a(b) = -\frac{1}{2} b^2 + \frac{7}{128} b^4 - \frac{29}{2304} b^6 + \frac{19}{5221} b^8 + \dots \tag{14}$$

The perturbation result of McLachlan is given by

$$a(b) = -\frac{1}{2} b^2 + \frac{7}{128} b^4 - \frac{29}{2304} b^6 + \frac{68687}{18874368} b^8 + \dots \tag{15}$$

The two expressions differ beginning in the 8th order term and the difference is only in the 9th decimal place.

When $d \neq 0$, the system is not Hamiltonian so that the stability boundaries must be found from $\det(\mathbf{I} \pm \mathbf{H}(a, b)) = 0$ (for flip and fold bifurcations, respectively). For $d = 0.31623$, the $\mathbf{O}(a^{18}b^{18})\mathbf{H}(a, b)$ matrix was computed and the corresponding stability boundaries are shown in Figure 2 within the vicinity of the primary 2 : 1 resonance. It is seen that, while the fold bifurcation curve through the origin appears to have retained the same shape as the corresponding one for the undamped system, the unstable flip bifurcation regions no longer

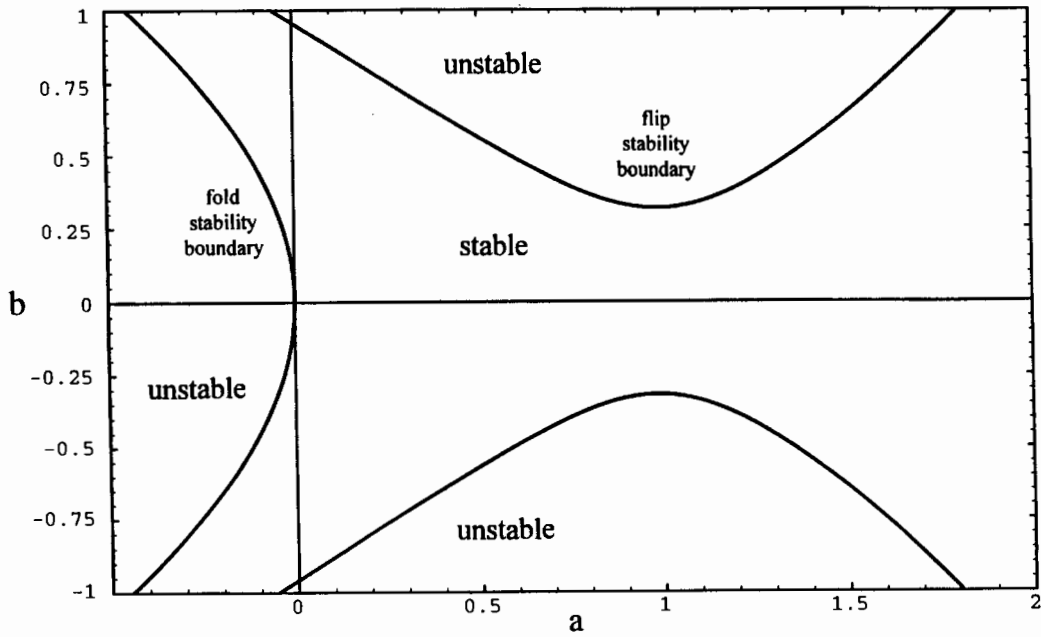


Figure 2. Stability boundaries for the damped ($d = 0.31623$) parametrically excited pendulum in the vicinity of the primary 2 : 1 resonance.

intersect the a axis and have ‘lifted up’. This feature of the damped system is well documented by Newland [15]. Even the curve through the origin is slightly altered with the addition of damping. This can be verified by computing the perturbation expansion coefficients of this curve using Equation (13), as before. The results are provided in Table 2 and differ slightly from the undamped perturbation coefficients. This may also be seen by computing the Floquet transition matrix with damping included as a third parameter. Since the relation $\det(\mathbf{I} - \mathbf{H}(a, b, d)) = 0$ for fold bifurcation results in homogeneous polynomials in a, b , and d , two approaches may again be used to graph the resulting two-dimensional surface. One is to substitute values of two of the parameters (say b and d) and solve the resulting polynomial equations for a to obtain a list of points which is then

$$a(b, d) = \sum_{i=0}^q \sum_{j=0}^q a_{ij} b^i d^j \tag{16}$$

used to fit a surface. The other approach is to use the double series expansion where a_{00} is a $b = d = 0$ bifurcation point on the a axis and the other a_{ij} coefficients are to be determined. When Equation (16) is substituted into the polynomial equation for fold bifurcation and like powers of b and d are collected, one obtains $q^2 + 2q$ linear equations which may be solved successively for the a_{ij} coefficients. Equation (16) then yields the bifurcation surface which is valid only for small values of b and d since this is equivalent to a perturbation expansion. When this was done up to the fourth order in b and d for the fold bifurcation at $a_{00} = 0$, the resulting surface expressed in rational fraction form was found to be

$$a(b, d) = -\frac{1}{2} b^2 + \frac{7}{128} b^4 + \left(\frac{1}{8} b^2 - \frac{29}{535} b^4 \right) d^2 + \left(-\frac{1}{32} b^2 + \frac{36}{1153} b^4 \right) d^4 + \dots \tag{17}$$

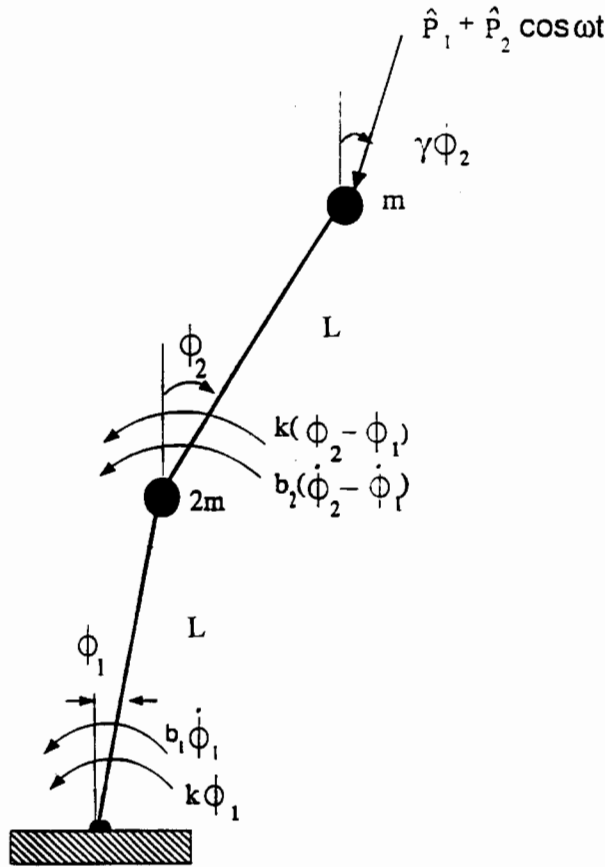


Figure 3. A double inverted pendulum with a periodic follower force.

4.2. A DOUBLE INVERTED PENDULUM WITH A PERIODIC FOLLOWER FORCE

As an example of a higher order system, consider the damped double inverted pendulum of Figure 3 subjected to a follower force with both constant and periodically-varying components. The time-periodic equations of motion for this system (the time-invariant form of which has been treated by Leipholz [16] and Herrmann [17]) may be expressed as

$$\begin{aligned}
 & 3\ddot{\phi}_1 + \cos(\phi_2 - \phi_1)\ddot{\phi}_2 - \sin(\phi_2 - \phi_1)\dot{\phi}_2^2 + (B_1 + B_2)\dot{\phi}_1 \\
 & \quad - B_2\dot{\phi}_2 + 2\bar{k}\phi_1 - \bar{k}\phi_2 - \bar{p}(t)\sin(\phi_1 - \gamma\phi_2) = 0, \\
 & \cos(\phi_2 - \phi_1)\ddot{\phi}_1 + \ddot{\phi}_2 + \sin(\phi_2 - \phi_1)\dot{\phi}_1^2 - B_2\dot{\phi}_1 + B_2\dot{\phi}_2 \\
 & \quad - \bar{k}\phi_1 + \bar{k}\phi_2 - \bar{p}(t)\sin((1 - \gamma)\phi_2) = 0,
 \end{aligned} \tag{18}$$

where $\bar{k} = k/ml^2$ is the normalized stiffness, $B_1 = b_1/ml^2$ and $B_2 = b_2/ml^2$ are the normalized damping constants, $\bar{p}(t) = (\hat{P}_1 + \hat{P}_2 \cos \omega t)/ml = P_1 + P_2 \cos \omega t$ is the normalized applied load, γ is the load direction parameter, and ω is the driving frequency of the applied load. Denoting $\mathbf{x}^T = (x_1 \ x_2 \ x_3 \ x_4) = (\phi_1 \ \phi_2 \ \dot{\phi}_1 \ \dot{\phi}_2)$ as the state vector and expanding Equation (18) in a Taylor series about the vertical $\phi_1 = \phi_2 = 0$ equilibrium position, the

above equation may be written in state space form as

$$\begin{pmatrix} \dot{x}_1 \\ \dot{x}_2 \\ \dot{x}_3 \\ \dot{x}_4 \end{pmatrix} = \begin{bmatrix} 0 & 0 & 1 & 0 \\ 0 & 0 & 0 & 1 \\ (-3\bar{k} + \bar{p}(t))/2 & \bar{k} - \bar{p}(t)/2 & -B_1/2 - B_2 & B_2 \\ (5\bar{k} - \bar{p}(t))/2 & -2\bar{k} + (3/2 - \gamma)\bar{p}(t) & B_1/2 + 2B_2 & -2B_2 \end{bmatrix} \\ \times \begin{pmatrix} x_1 \\ x_2 \\ x_3 \\ x_4 \end{pmatrix} + \begin{pmatrix} 0 \\ 0 \\ f_{33}(\mathbf{x}, t) \\ f_{34}(\mathbf{x}, t) \end{pmatrix};$$

$$f_{33}(\mathbf{x}, t) = \frac{1}{2} (x_2 - x_1)(x_3^2 + x_4^2) - \frac{1}{12} \bar{p}(t)[x_1 - \gamma x_2]^3 - (1 - \gamma)^3 x_2^3 \\ + \frac{1}{4} (x_2 - x_1)^2 [(4\bar{k} - \bar{p}(t))x_1 + (-3\bar{k} + (2 - \gamma)\bar{p}(t))x_2 \\ + (B_1 + 3B_2)x_3 - 3B_2x_4];$$

$$f_{34}(\mathbf{x}, t) = -\frac{1}{2} (x_2 - x_1)(3x_3^2 + x_4^2) + \frac{1}{12} \bar{p}(t)[(x_1 - \gamma x_2)^3 - 3(1 - \gamma)^3 x_2^3] \\ + \frac{1}{4} (x_2 - x_1)^2 [(-7\bar{k} + 2\bar{p}(t))x_1 + (5\bar{k} + (\gamma - 3)\bar{p}(t))x_2 \\ - (2B_1 + 5B_2)x_3 + 5B_2x_4], \quad (19)$$

where terms up to the cubic order have been retained.

For the parameter set $\omega = 2$, $\bar{k} = 1$, and $B_1 = B_2 = 0$, the system is Hamiltonian and preserves volume in state space since $\text{tr}(\mathbf{A}(t, P_1, P_2, \gamma)) = 0$ (where $\mathbf{A}(t, P_1, P_2, \gamma)$ is the linear system matrix in Equation (19)) even though the nonconservative forces for $\gamma \neq 0$ cannot be derived from a potential. If $P_2 = 0$, then the system is time-invariant so that the stability and bifurcation boundaries may be extracted directly from $\mathbf{A}(P_1, \gamma)$ using the standard Routh–Hurwitz criteria. These well-known results are reproduced in Figure 4A in which the tangent bifurcation lines in the (P_1, γ) plane represent the boundaries of regions in which the physical system fails due to divergence or buckling to another equilibrium position while the egg-shaped Krein collision region represents dynamic failure due to flutter [16, 17]. Since all four eigenvalues must participate in a Krein collision, this region cannot overlap with that due to tangent bifurcation. When damping is added, the tangent bifurcation boundaries (now fold) remain unaffected since divergence is a static failure mode, while those corresponding to Hopf bifurcation are now able to cross into the fold bifurcation regions since only two eigenvalues are required. This is shown in Figure 4B where the damping values are $B_1 = B_2 = 0.01$. It can be seen in these figures that tangent or fold bifurcation is not possible in a certain range of the load direction parameter ($0.556 < \gamma < 1$) and that the Krein collision or Hopf bifurcation only occurs in another region ($0.345 < \gamma < 1.30$) which overlaps that of tangent and fold bifurcations, respectively.

In the following, bifurcation relations for the time-periodic ($P_2 \neq 0$) undamped and damped system are plotted in the (P_1, P_2) plane for load direction values of $\gamma = 0$ (when the load is vertical and thus conservative) and $\gamma = 1$ (when the load is tangential to the top

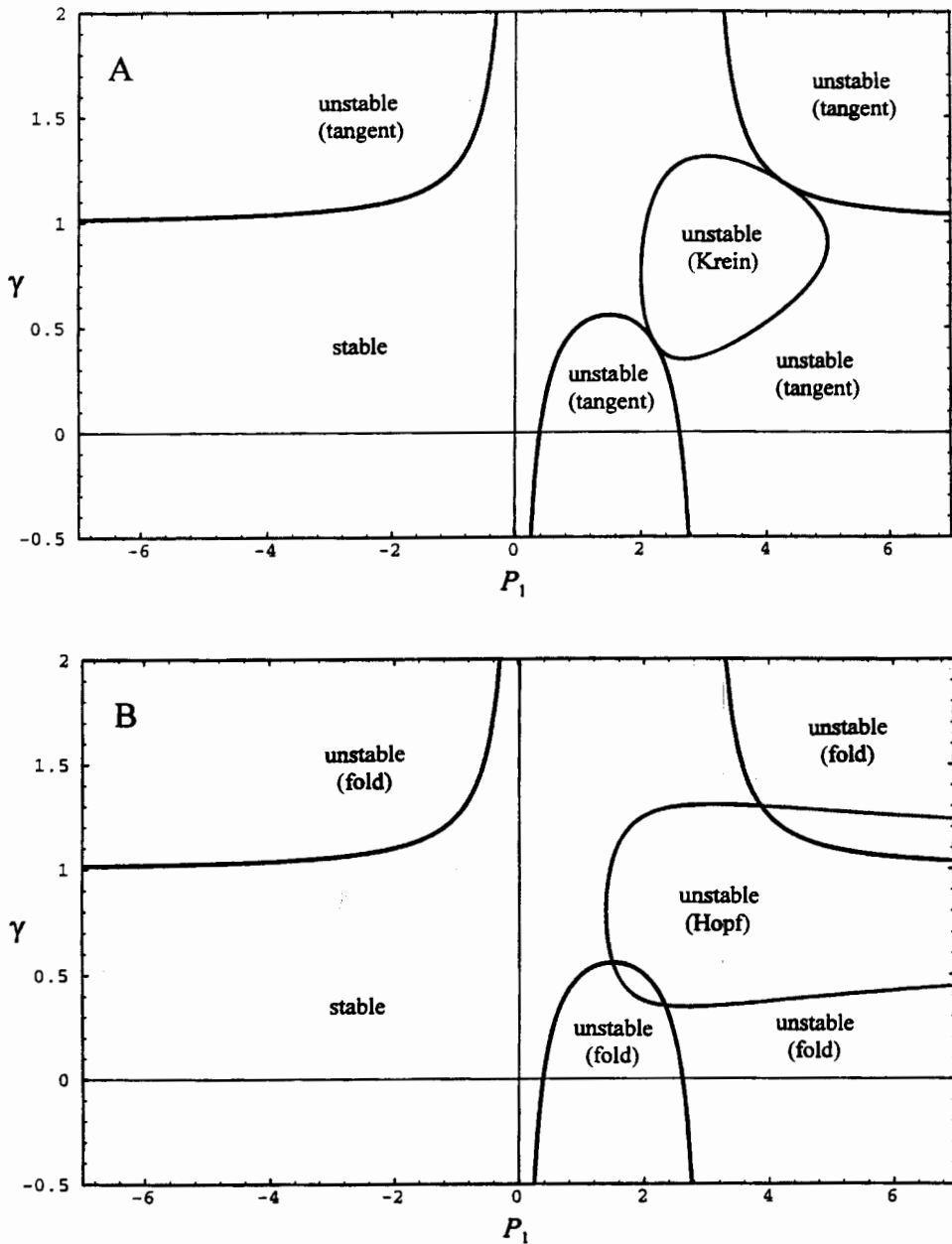


Figure 4. Bifurcation diagrams of the time-invariant ($P_2 = 0$) double inverted pendulum in the (P_1, γ) plane for (A) $B_1 = B_2 = 0$ and (B) $B_1 = B_2 = 0.01$.

link and thus nonconservative). While the explicit FTMs are not reported, in each case they were obtained using $(p, m) = (34, 18)$ and are of order $O(P_1^p P_2^m)$ where $P = p/2 = 17$. The required *cpu* times averaged roughly 14 hours while 128 MB of RAM provided sufficient memory in each case. For more information on how the *cpu* time varies with the number of iterations in this problem, see [6].

Figure 5 shows the stability diagram of the undamped $B_1 = B_2 = 0$ system for $\gamma = 0$ obtained by both symbolic computation of the FTM and by direct numerical integration over

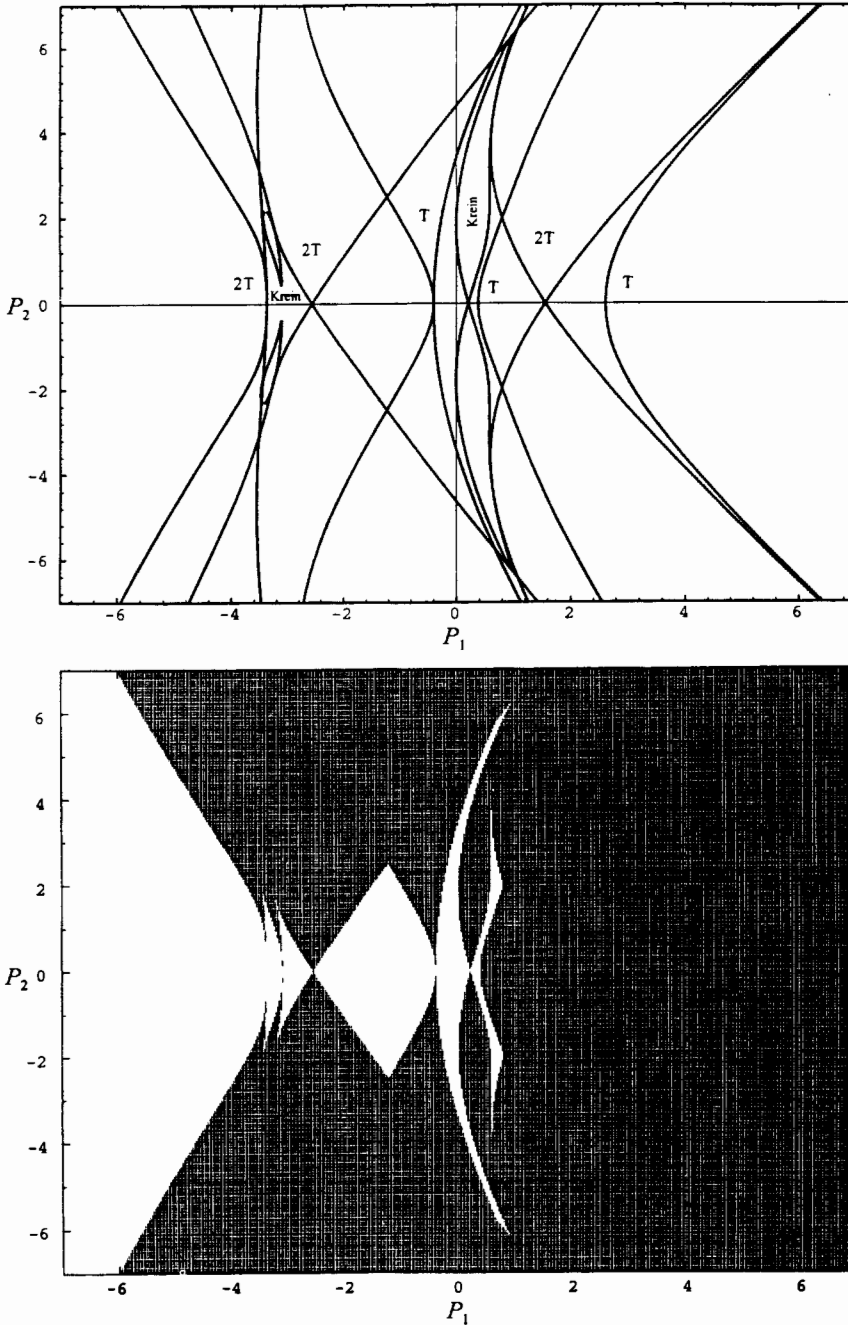


Figure 5. Symbolic and numerical bifurcation diagrams in the (P_1, P_2) plane for the double inverted pendulum with $B_1 = B_2 = 0$ and $\gamma = 0$. The white regions in the numerical diagram are stable and the black regions are unstable.

one period for 217,156 points in the (P_1, P_2) plane. The determinant of the FTM ($1.0 + O(10^{-7})$) is very close to unity, thus indicating that phase space volume is conserved. The conditions

$$\begin{aligned} \det(\mathbf{I} - \mathbf{H}(\boldsymbol{\alpha})) &= 2 - 2c_1(\boldsymbol{\alpha}) + c_2(\boldsymbol{\alpha}) = 0; \\ \det(\mathbf{I} + \mathbf{H}(\boldsymbol{\alpha})) &= 2 + 2c_1(\boldsymbol{\alpha}) + c_2(\boldsymbol{\alpha}) = 0; \\ c_1^2(\boldsymbol{\alpha}) - 4c_2(\boldsymbol{\alpha}) + 8 &= 0; \quad \boldsymbol{\alpha} = (P_1, P_2) \end{aligned} \tag{20}$$

for tangent, period-doubling, and Krein collision (Hamiltonian Hopf) bifurcations, respectively, were used where $c_i(\boldsymbol{\alpha})$ are coefficients of the FTM's characteristic polynomial of $\mathbf{H}(\boldsymbol{\alpha})$ given by

$$\det(\mathbf{H}(\boldsymbol{\alpha}) - \mu\mathbf{I}) = \mu^4 - c_1(\boldsymbol{\alpha})\mu^3 + c_2(\boldsymbol{\alpha})\mu^2 - c_3(\boldsymbol{\alpha})\mu + c_4(\boldsymbol{\alpha}). \tag{21}$$

These relations were obtained by using the standard linear fractional transformation to map the unit circle of the complex plane into the left half plane [18] followed by application of the Routh–Hurwitz criteria while using the simplifications $c_1(\boldsymbol{\alpha}) = c_3(\boldsymbol{\alpha})$ and $c_4(\boldsymbol{\alpha}) = 1$ which result from all four multipliers lying on the unit circle [19]. The Schur–Cohn criteria [20] for discrete systems may also be used which yields identical results. In Figure 5, the two tangent bifurcation lines in the right half of the diagram (the leftmost of which represents a stability boundary) intersect the $P_2 = 0$ line at the same location ($P_1 = 0.38197$ and 2.61803) as in Figure 4A for $\gamma = 0$. In addition to these, there are three period-doubling regions, two Krein collisions, and an additional tangent bifurcation region, all of which are symmetric about the $P_2 = 0$ line which they intersect at a single point $P_1 = -3.3756, -3.1, -2.56155, -0.39672, 0.21032,$ and 1.56155 . All of these lines contribute to the overall stability boundary shown in the numerically-obtained diagram in which the white regions are stable and the black regions are unstable. The Krein collision regions may not overlap with other unstable regions in this case since all four eigenvalues are required. It can be seen that the stable white regions ‘open up’ to the left for negative P_1 as one would expect.

Figure 6 shows the stability diagram of the damped $B_1 = B_2 = 0.01$ system for $\gamma = 0$ also obtained by both symbolic computation of the FTM (with the same parameters as before) and by direct numerical integration. Once again applying the linear fractional transformation to Equation (21) followed by application of the Routh–Hurwitz criteria, the conditions

$$\begin{aligned} \det(\mathbf{I} - \mathbf{H}(\boldsymbol{\alpha})) &= 1 - c_1(\boldsymbol{\alpha}) + c_2(\boldsymbol{\alpha}) - c_3(\boldsymbol{\alpha}) + c_4(\boldsymbol{\alpha}) = 0; \\ \det(\mathbf{I} + \mathbf{H}(\boldsymbol{\alpha})) &= 1 + c_1(\boldsymbol{\alpha}) + c_2(\boldsymbol{\alpha}) + c_3(\boldsymbol{\alpha}) + c_4(\boldsymbol{\alpha}) = 0; \\ (1 - c_4(\boldsymbol{\alpha}))^2(1 + c_4(\boldsymbol{\alpha}) - c_2(\boldsymbol{\alpha})) &+ (c_1(\boldsymbol{\alpha}) - c_3(\boldsymbol{\alpha}))(c_3(\boldsymbol{\alpha}) - c_1(\boldsymbol{\alpha})c_4(\boldsymbol{\alpha})) = 0 \end{aligned} \tag{22}$$

for fold, flip, and secondary Hopf bifurcations, respectively, were obtained. These relations can also be found in [12, 19, 21]. The two fold bifurcation lines, which correspond to those in Figure 4B, intersect the $P_2 = 0$ line at the same places as before. While many of the unstable regions appear to have ‘lifted up’ as in the case of the damped Mathieu Equation, intersections with the $P_2 = 0$ line occurs for two flip regions (at the same locations as in the undamped equation) and one of the secondary Hopf regions which now intersects at $P_1 = 0.20808$. The overlapping of this region with other unstable regions is now possible since only two eigenvalues are required and this effectively removes part of the narrow stable regions in Figure 5.

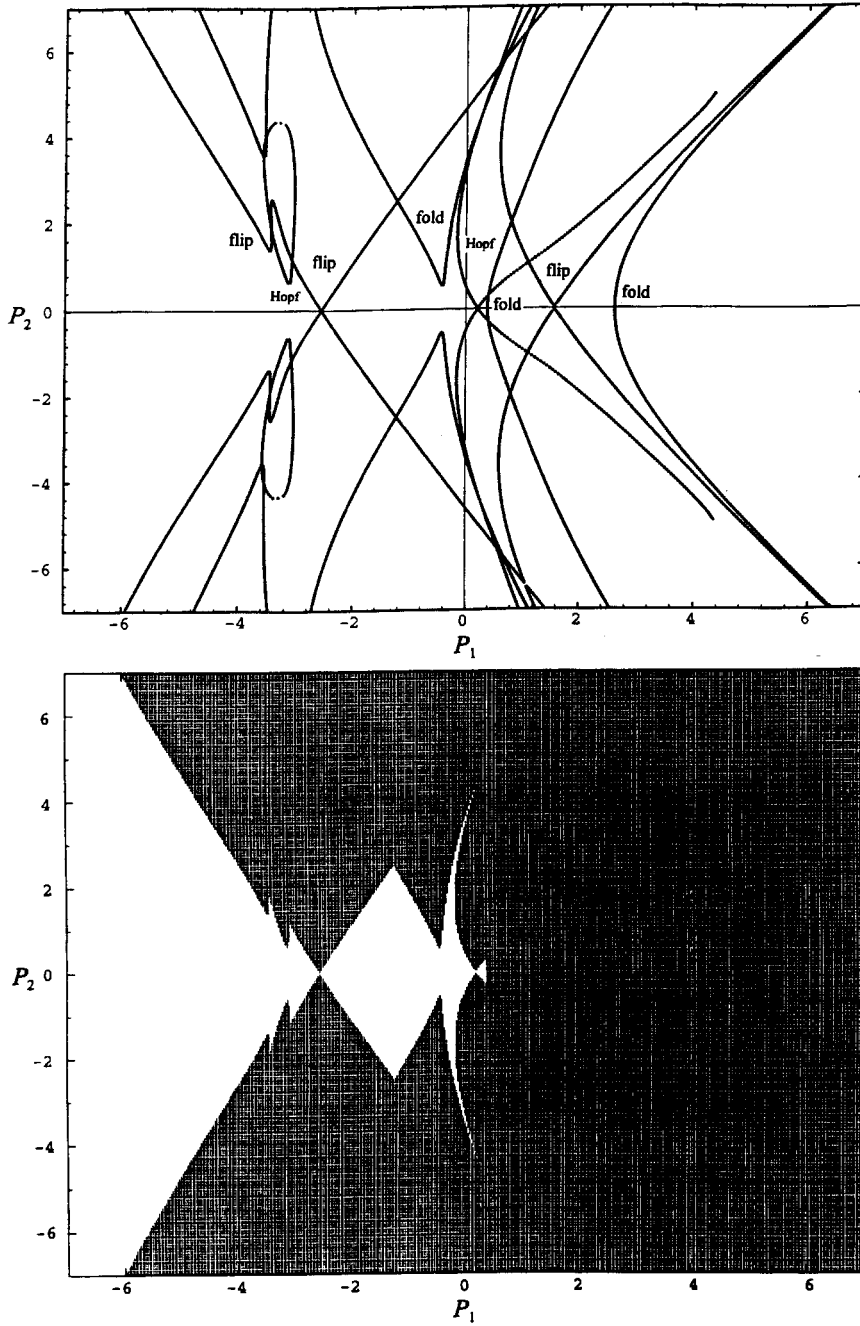


Figure 6. Symbolic and numerical bifurcation diagrams in the (P_1, P_2) plane for the double inverted pendulum with $B_1 = B_2 = 0.01$ and $\gamma = 0$.

When the loading angle is completely tangential, the bifurcation diagrams are simplified by the fact that tangent or fold bifurcations to another static equilibrium cannot occur. Figure 7 shows the stability diagram of the undamped $B_1 = B_2 = 0$ system for $\gamma = 1$ again obtained by both symbolic computation of the FTM and by direct numerical integration. The conditions given by Equation (20) were used to find the period-doubling and Krein collision boundaries at which dynamic failure due to flutter occurs. The two Krein collision lines on the right half side of the diagram correspond to the intersections at $\gamma = 1$ in Figure 4A which occur at $P_1 = 2.08579$ and 4.91421 . In addition, there are two period-doubling regions and another Krein collision region which meet the $P_2 = 0$ line at a single point at $P_1 = -5.55556, -1.9142, \text{ and } 2$. A very small stable region is situated between the $P_1 = 2$ period-doubling region and the $P_1 = 2.08579$ Krein collision region which cannot overlap.

In Figure 8, the equivalent damped system with $B_1 = B_2 = 0.01$ and $\gamma = 1$ is shown in which the relations in Equation (22) were used again to find the flip and secondary Hopf bifurcation boundaries. It is seen, in contrast to Figure 7, that only one of the right half side secondary Hopf bifurcation lines is present and that it has moved to the left with a $P_2 = 0$ intersection at $P_1 = 1.46434$. This also agrees with the results shown in Figure 4B in which the rightmost boundary has effectively moved to infinity. In addition, overlapping with the nearest flip bifurcation region occurs.

As in the previous example, the symbolic procedure may be used in conjunction with a series expansion in terms of the periodic parameter. For this purpose, P_1 is expanded in P_2 as

$$P_1(P_2) = P_{10} + \sum_{i=1}^q P_{1i} P_2^i, \tag{23}$$

where P_{10} is a $P_2 = 0$ bifurcation point on the P_1 axis and P_{1i} are the expansion coefficients to be determined. Equation (23) may be substituted into the appropriate expression in Equation (20) or (22) from which one obtains q Equations in the unknown coefficients P_{1i} after collecting like powers of P_2 . The resulting expressions are given to eighth order for the tangent (fold) bifurcation routes at $P_{10} = 0.38197$ and $P_{10} = 2.61803$ for $\gamma = 0$.

$$\begin{aligned} P_1(P_2) &= 0.38197 + 0.19656P_2^2 - 0.067452P_2^4 + 0.040256P_2^6 - 0.029521P_2^8 + \dots, \\ P_1(P_2) &= 2.61803 + 0.13103P_2^2 - 0.002874P_2^4 \\ &\quad + 0.0000892P_2^6 - 3.8377 \times 10^{-9}P_2^8 + \dots. \end{aligned} \tag{24}$$

For $\gamma = 1$ Krein collision and secondary Hopf routes at $P_{10} = 2.08579, 4.91421, \text{ and } 1.46434$ for $B_1 = B_2 = 0.0, 0.0, \text{ and } 0.01$, respectively. They are given as

$$\begin{aligned} P_1(P_2) &= 2.08579 + 0.86649P_2^2 - 0.99781P_2^4 + 2.16508P_2^6 - 5.79223P_2^8 + \dots, \\ P_1(P_2) &= 4.91421 + 0.07106P_2^2 - 0.0005105P_2^4 + 7.4842 \times 10^{-6}P_2^6 \\ &\quad - 1.3481 \times 10^{-7}P_2^8 + \dots, \\ P_1(P_2) &= 1.46434 + 7.88857P_2^2 - 224.34P_2^4 + 11128.1P_2^6 - 675088P_2^8 + \dots. \end{aligned} \tag{25}$$

Of these five expressions, the expansions that converge faster are valid over larger intervals in P_2 . The fact that these results can be obtained relatively easily using the symbolic procedure is highly significant since use of the perturbation method to obtain them directly for this two-degree-of-freedom system would be rather difficult.

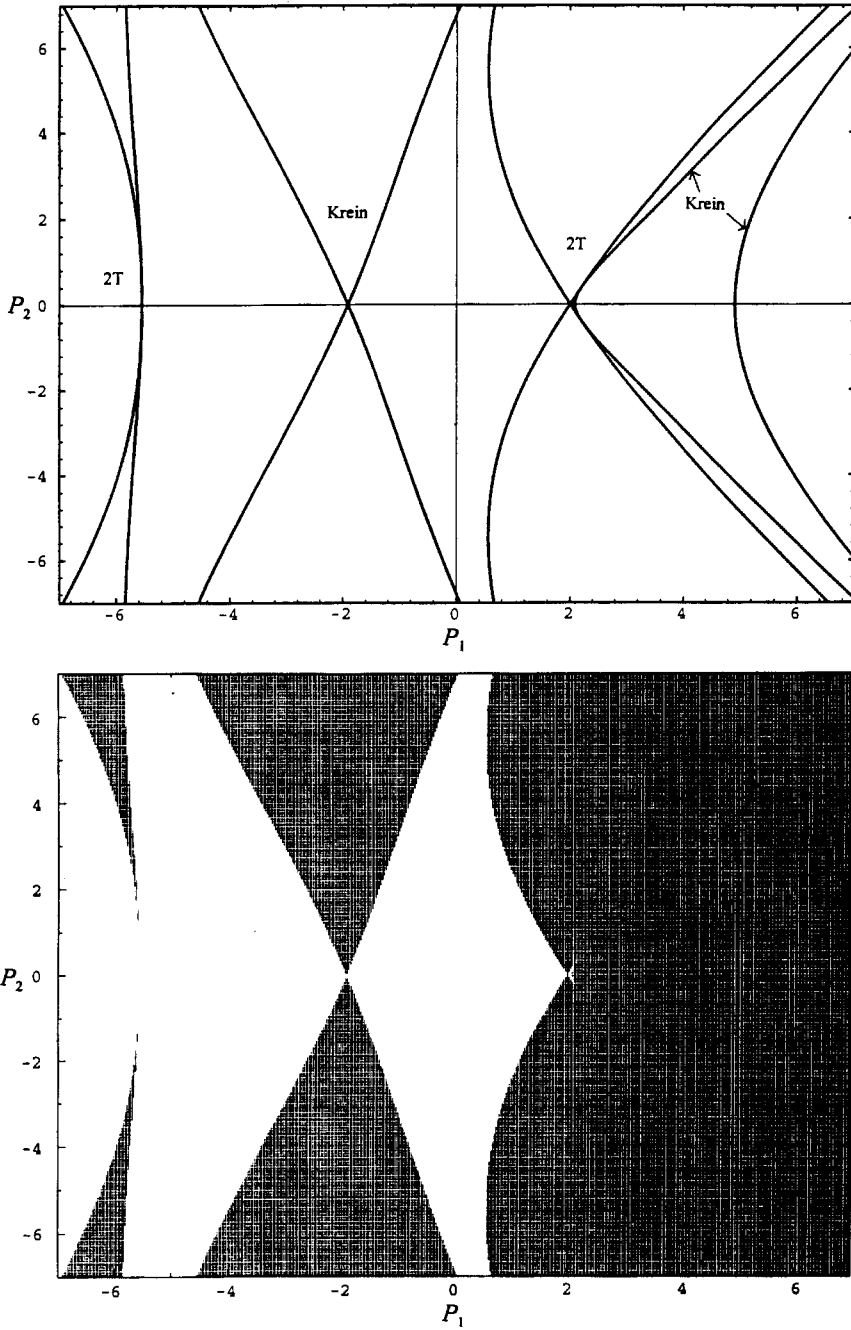


Figure 7. Symbolic and numerical bifurcation diagrams in the (P_1, P_2) plane for the double inverted pendulum with $B_1 = B_2 = 0$ and $\gamma = 1$.

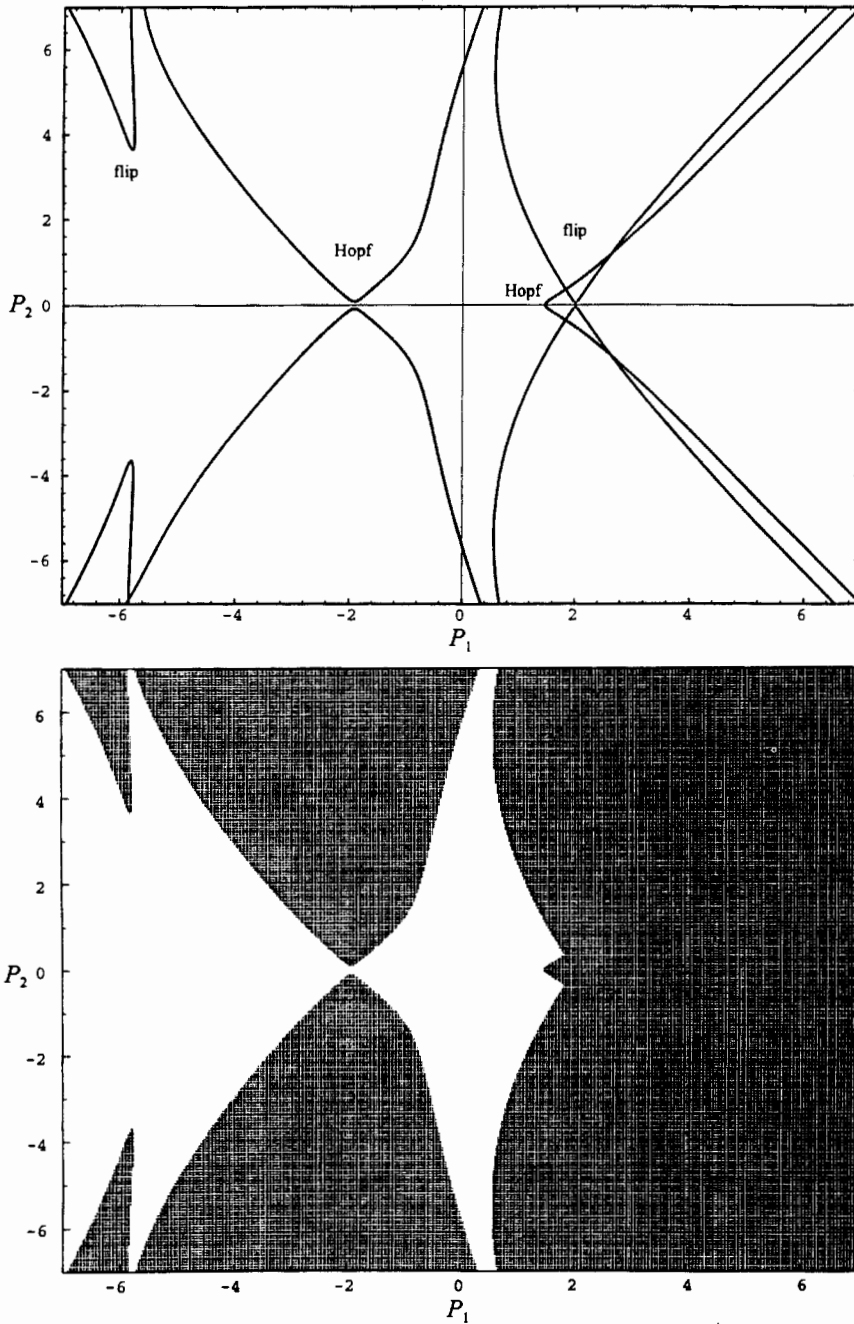


Figure 8. Symbolic and numerical bifurcation diagrams in the (P_1, P_2) plane for the double inverted pendulum with $B_1 = B_2 = 0.01$ and $\gamma = 1$.

5. Conclusions

A new technique for the symbolic computation of local stability boundaries and bifurcation surfaces for nonlinear time-periodic dynamical systems explicitly as a function of system parameters has been presented. This technique is applicable to multidimensional systems and utilizes a recently developed symbolic computational algorithm for approximating the parameter-dependent fundamental solution matrix of linear time-periodic systems. By evaluating this matrix at the end of the principal period, the parameter-dependent Floquet transition matrix (FTM), or the linear part of the Poincaré map, was obtained. Subsequently, the well-known criteria for local stability and bifurcation conditions of equilibria and periodic solutions were applied to determine the Equations for the bifurcation surfaces in the parameter space as homogeneous polynomials of the system parameters. Because this method is *not* based on expansion in terms of a small parameter, it can successfully be applied to periodic systems whose internal excitation is strong. While the proposed method may be more efficient in terms of *cpu* time than the truncated point mapping method, it is probably more expensive in terms of the memory requirement. A parametrically excited simple pendulum and a double inverted pendulum subjected to a periodic follower force were included as illustrative examples. The equations for the bifurcation surfaces in the parameter space were obtained and plotted for a variety of different parameter sets. By constructing a series expansion in one or two parameters, perturbation results were either rederived or obtained for the first time.

Acknowledgment

Financial support for this work was provided by the Army Research Office, monitored by Dr. Gary L. Anderson under contract number DAAH04-94G-0337.

References

1. Nayfeh, A. H., *Perturbation Methods*, Wiley, New York, 1973.
2. Sanders, J. A. and Verhulst, F., *Averaging Methods in Nonlinear Dynamical Systems*, Springer-Verlag, New York, 1985.
3. Lindt, K. G. and Likins, P. W., 'Infinite determinant methods for stability analysis of periodic-coefficient differential equations', *AIAA Journal* **8**, 1970, 680–686.
4. Guttalu, R. S. and Flashner, H., 'Analytical study of stability of periodic systems by Poincaré mappings', in *Vibration of Nonlinear, Random, and Time-Varying Systems*, Proceedings of the 1995 Design Engineering Technical Conferences, Boston, MA, September 17–21, S. C. Sinha, J. P. Cusumano, and F. Pfeiffer (eds.), Vol. 3-A, DE Vol. 84-1, 1995, pp. 387–398.
5. Guttalu, R. S. and Flashner, H., 'Stability analysis of periodic systems by truncated point mappings', *Journal of Sound and Vibration* **189**, 1996, 33–54.
6. Sinha, S. C. and Butcher, E. A., 'Symbolic computation of fundamental solution matrices for time-periodic dynamical systems', *Journal of Sound and Vibration* **206**(1), 1997, 61–85.
7. Sinha, S. C. and Wu, D.-H., 'An efficient computational scheme for the analysis of periodic systems', *Journal of Sound and Vibration* **151**, 1991, 91–117.
8. Pandiyan, R. and Sinha, S. C., 'Analysis of time-periodic nonlinear dynamical systems undergoing bifurcations', *Nonlinear Dynamics* **8**, 1995, 21–43.
9. Yakubovich, V. A. and Starzhinskii, V. M., *Linear Differential Equations with Periodic Coefficient*, Part I and Part II, Wiley, New York, 1975.
10. Arrowsmith, D. K. and Place, C. M., *An Introduction to Dynamical Systems*, Cambridge University Press, Cambridge, 1990.
11. Lichtenberg, A. J. and Leiberman, M. A., *Regular and Chaotic Dynamics*, Springer-Verlag, New York, 1992.

12. Flashner, H. and Hsu, C. S., 'A study of nonlinear periodic systems via the point mapping method', *International Journal for Numerical Methods in Engineering* **19**, 1983, 185–215.
13. Bogoliubov, N. N. and Mitropolsky, J. A., *Asymptotic Methods in the Theory of Nonlinear Oscillations*, State Press for Physics and Mathematical Literature, Moscow, 1963 [in Russian]. English translation: Hindustan Publishing Co., Delhi, India/Gordon and Breach, New York.
14. McLachlan, N. W., *Theory and Application of Mathieu Functions*, Clarendon Press, Oxford, 1947.
15. Newland, D. E., *Mechanical Vibration Analysis and Computation*, Wiley, New York, 1989.
16. Leipholz, H., *Stability Theory*, Academic Press, New York, 1970.
17. Herrmann, G., 'Dynamics and stability of mechanical systems with follower forces', NASA contractor report No. NASA CR-1782, prepared by Stanford University, 1971.
18. Jury, E. I., *Inners and Stability of Dynamic Systems*, Wiley-Interscience, New York, 1974.
19. Carcasses, J.-P., 'A necessary and sufficient condition to have r pairs of complex multipliers with modulus equal to unity in the case of an n -dimensional map', *International Journal of Bifurcation and Chaos* **5**(4), 1995, 1193–1204.
20. Kuo, B. C., *Analysis and Synthesis of Sampled-Data Control Systems*, Prentice Hall, Englewood Cliffs, NJ, 1963.
21. Kawakami, H., 'Bifurcation of periodic responses in forced dynamic nonlinear circuits: Computation of bifurcation values of the system parameters', *IEEE Transactions on Circuits and Systems* **CAS-31**, 1984, 248–260.